




## RESEARCH ARTICLE

# Single-particle analysis of circulating bacterial extracellular vesicles reveals their biogenesis, changes in blood and links to intestinal barrier

Zihao Ou<sup>1</sup>  | Bo Situ<sup>1</sup> | Xinyue Huang<sup>1,2</sup> | Yicong Xue<sup>1</sup> | Xiaojing He<sup>1</sup> | Qianbei Li<sup>1</sup> | Dejin Ou<sup>3</sup> | Bairong He<sup>1</sup> | Jing Chen<sup>1</sup> | Yiyao Huang<sup>1</sup> | Lulu Deng<sup>4</sup> | Mingying Zhang<sup>1</sup> | Qian Wang<sup>1,2</sup>  | Lei Zheng<sup>1</sup> 

<sup>1</sup>Department of Laboratory Medicine, Nanfang Hospital, Southern Medical University, Guangzhou, China

<sup>2</sup>Zhujiang Hospital, Southern Medical University, Guangzhou, China

<sup>3</sup>Department of Laboratory Medicine, The Third Affiliated Hospital of Guangzhou Medical University, Guangzhou, China

<sup>4</sup>Medical Laboratory Center, Guangzhou Red Cross Hospital, Guangzhou, China

## Correspondence

Bo Situ, Qian Wang and Lei Zheng, Department of Laboratory Medicine, Nanfang Hospital, Southern Medical University, Guangzhou, 510515, China.  
Email: bositu@smu.edu.cn, wangqian@smu.edu.cn and nfyzhenglei@smu.edu.cn

## Funding information

The Outstanding Youths Development Scheme of Nanfang Hospital, Southern Medical University, Grant/Award Number: 2022J001; National Key R&D Program of China, Grant/Award Number: 2021YFA1300604; The Natural Science Foundation of Guangdong Province, Grant/Award Numbers: 2021A151011639, 2023A151012512; The National Science Fund for Distinguished Young Scholars, Grant/Award Number: 82025024; The National Natural Science Foundation of China, Grant/Award Numbers: 82302593, 82272438, 82002245; The Major State Basic Research Development Program of Natural Science Foundation of Shandong Province in China, Grant/Award Number: ZR2020ZD11; The Post-doctoral Science Foundation, Grant/Award Number: 2022M720059

## Abstract

Bacterial extracellular vesicles (BEVs) are nano-size particles secreted by bacteria that carry various bioactive components. These vesicles are thought to provide a new window into the mechanisms by which bacteria affect their hosts, but their fundamental properties within human remain poorly understood. Here, we developed a single-vesicle analytical platform that enabled BEV detection in complex biological samples of host. Using this platform, we found the presence of BEVs in the host circulation and they were mainly derived from gut microbes. We showed that the levels of circulating BEVs in humans significantly increased with aging due to an age-related increase in intestinal permeability. Significantly different levels of BEVs in blood were also found in patients with colorectal cancer and colitis. Together, our study provides new insights into circulating BEV biology and reveals their potential as a new class of biomarkers.

## KEYWORDS

bacterial extracellular vesicles, biomarkers, single-particle

## 1 | INTRODUCTION

The human gut is colonized by a huge number of bacteria (Han et al., 2022; Lee et al., 2022). In the past decade, advances in high-throughput sequencing methodology have allowed researchers to analyze the bacterial composition of the gut and demonstrated their important roles in human health (Sergey et al., 2022; Tan et al., 2022). The imbalance of the resident bacterial communities is closely linked to a wide variety of diseases including colitis (Atreya & Siegmund, 2021), cancer (Møller et al., 2022), hypertension

Zihao Ou and Bo Situ contributed equally to this study.

This is an open access article under the terms of the [Creative Commons Attribution-NonCommercial-NoDerivs License](https://creativecommons.org/licenses/by-nc-nd/4.0/), which permits use and distribution in any medium, provided the original work is properly cited, the use is non-commercial and no modifications or adaptations are made.

© 2023 The Authors. *Journal of Extracellular Vesicles* published by Wiley Periodicals LLC on behalf of International Society for Extracellular Vesicles.

(Tang et al., 2019) and Alzheimer's disease (Ou et al., 2020). Gut microbiota is therefore commonly viewed as a new window into pathogenesis of diseases as well as a promising therapeutic target (Hod & Ringel, 2016). However, most of these findings come from the correlative studies (Fassarella et al., 2021; Frost et al., 2021). The underlying mechanisms by which bacteria affect their hosts, especially how bacteria affect distant organs outside the gut, are largely unclear.

Identification of the components released by the bacteria is a key approach to investigate their specific functions. Among the substances secreted by bacteria, bacterial extracellular vesicles (BEVs) have drawn substantial attention due to their unique roles (Erttmann et al., 2022; Wen et al., 2023). BEVs are nanoscale vesicles (20–250 nm) with lipid bilayer that are naturally released by bacteria (Kaparakis-Liaskos & Ferrero, 2015; Toyofuku et al., 2019). These vesicles contain various components including lipids, proteins, and nucleic acids from their mother bacteria (Chen et al., 2022). By delivering these molecular cargos, BEVs participate in a wide range of bacterial communications such as the interception of bacteriophages and antibiotics, the transfer of virulence factors and resistant gene (Janda & Robatzek, 2022; Jiang et al., 2022). In addition, BEVs are involved in many physiological and pathological conditions of the host intestinal tract (Gul et al., 2022). For example, *Helicobacter pylori*-derived BEVs induce T cell apoptosis, contributing to dysregulation both proinflammatory and anti-inflammatory processes (Turner et al., 2018); *Akkermansia muciniphila*-derived BEVs promote intestinal cells to secrete mucus, thereby maintaining intestinal function balance (Ashrafi et al., 2019). Notably, recent studies have shown that BEVs can be found in human plasma (Tulkens et al., 2020) and peripheral tissues after gavage feeding in mouse. In view of the properties that EVs of host origin, such as exosomes and apoptotic bodies could deliver cargo over long distances (Bittel et al., 2021; Cecil et al., 2019), these studies raised an intriguing possibility that BEVs with similar structure and size to host EVs may be new mediators of long-distance bacteria-host interactions through the bloodstream. However, many important questions of blood BEVs remain to be answered. Where the BEVs in the blood come from and the underlying mechanisms that cause BEVs to be released into the host circulation remain unknown. The biological and clinical significance of circulating BEVs have yet to be investigated. Answering these fundamental questions require new tools to further explore their roles and functions.

Here, we identified specific markers that enable BEVs to be well-distinguished from host-derived EVs. In combination with nano-flow cytometry (nFCM) analyses, we further explored their source, release mechanism, and changes in the blood level during the human lifespan. The clinical values of BEVs in patients with intestinal diseases were also revealed. Collectively, this study improves our understanding of circulating BEVs and provides new insights into their changes in health and diseases.

## 2 | MATERIALS AND METHODS

### 2.1 | Clinical information of healthy donors and patient population

The sample collection protocol was approved by the Ethics Committee of Nanfang Hospital, Southern Medical University (approval number: NFEC-2022-001). Healthy donors and patients with colitis and colon cancer were selected from Nanfang hospital and grouped according to standard guidelines (Amin et al., 2017; Carter et al., 2004). Data on patient demographics (age and gender), disease characteristics, current and previous treatments were collected. All serum samples were collected (1 mL) within 24 h and stored at  $-80^{\circ}\text{C}$ .

### 2.2 | Animal model

C57BL/6J mice, nude mice and germ-free (GF) mice were purchased from GemPharmatech Co., Ltd. We found no significant difference in circulating BEVs levels between males and females in human samples, so male mice were only used in subsequent experiments. All animal experiments were approved by the Committee on the Use of Live Animals in Teaching and Research at the Southern Medical University (approval number: SMUL2022002). For the colonization of mCherry *E. coli* in the gut, nude male mice were gavaged (4–5 weeks of age) with mCherry *E. coli* ( $10^9$  CFU/mL, 200  $\mu\text{L}/\text{day}$ ) for 15 days. For the construction of intestinal bacterial clearance model, a mixture of ampicillin (200 mg/mL, Sigma), vancomycin (100 mg/mL, Sigma), neomycin (200 mg/mL, Sigma), gentamycin (200 mg/mL, Sigma), and erythromycin (200 mg/mL, Sigma) was implanted in each C57BL/6J male mouse (4–6 weeks of age) for 7 days (200  $\mu\text{L}/\text{day}$ ). For the construction of intestinal barrier injury model, DSS (Sigma) was dissolved in water at a concentration of 3.0% (w/v) and oral administrated for 7 days.

### 2.3 | Culture of bacteria strains and isolation of BEVs

*Escherichia coli* (ATCC31617), *Klebsiella pneumoniae* (ATCC700603), *Pseudomonas aeruginosa* (ATCC29260), *Acinetobacter baumannii* (ATCC15308), *Staphylococcus aureus* (ATCC29740), *Enterococcus faecalis* (ATCC19433), *Streptococcus pneumoniae* (ATCC49619) and *Staphylococcus epidermidis* (ATCC12228) were obtained from the American Type Culture Collection (ATCC).

*Escherichia coli*, *Klebsiella pneumoniae*, *Pseudomonas aeruginosa* and *Acinetobacter baumannii* strains were cultured in Luria-Bertani (LB) media (sigma) and *Staphylococcus aureus*, *Enterococcus faecalis*, *Streptococcus pneumoniae* and *Staphylococcus epidermidis* strain were cultured in Brain Heart Infusion (BHI) media (sigma). mCherry *E. coli* was cultured in LB with kanamycin (100 µg/mL, Sigma). For BEV preparations, bacterial strains were grown at 37°C till OD600 of 0.4–0.5. Isolation of BEVs as described previously (Li et al., 2020). Briefly, supernatant was centrifuged at 1000 × g for 20 min and 10,000 × g for 30 min at 4°C, and further filtered through a 0.22 µm filter. This supernatant was pelleted twice using ultracentrifugation at 135,000 × g for 1.5 h at 4°C. BEVs were resuspended in 100 µL PBS after removing the supernatant and stored at –80°C.

## 2.4 | Cell culture and isolation of EVs

A549, 3T3-L1, MCF-7 and SMC cells were purchased from the ATCC. All cell lines were authenticated and were tested routinely before use to avoid mycoplasma contamination. A549, 3T3-L1, MCF-7 and SMC cells were grown in Dulbecco's Modified Eagle Medium (DMEM, Gibco) supplemented with 10% (v/v) Fetal Bovine Serum (FBS, Gibco). For EV preparations, all cell lines were cultured for 48 h. The supernatant was collected and centrifuged 300 × g for 20 min, 2000 × g for 20 min and 12,000 × g for 30 min at 4°C, and further pelleted twice using ultracentrifugation at 135,000 × g for 1.5 h at 4°C. EVs were resuspended in 100 µL PBS after removing the supernatant and stored at –80°C for subsequent studies.

## 2.5 | EV isolation from serum

Serum samples were centrifuged at 1000 × g for 10 min and 12,000 × g for 20 min at 4°C to eliminate cellular debris. Subsequently, samples underwent ultracentrifugation at 120,000 × g for 35 min at 4°C. The resulting pellet was washed with 4 mL of PBS and subjected to a second ultracentrifugation at 120,000 × g for 35 min at 4°C. The supernatant was discarded, and the EVs were resuspended in PBS. The EV suspension was stored at –80°C for subsequent studies. From 1 mL of serum sample, we isolated EVs with an approximate total protein content of 50–80 µg. The particle concentration was estimated to be  $8.1 \times 10^{10}$  particles/mL, yielding a particle-to-protein ratio of approximately  $1.0125 \times 10^{12}$  particles/mg.

## 2.6 | Isolation of fecal EVs by density gradient centrifugation

Fecal samples were aliquoted in pre-weighted 50 mL tubes and homogenized in PBS at a ratio of 10:1 (v/w, mL/g) with samples. The homogenate underwent low-speed centrifugation at 3000 × g for 20 min to remove cells, bacteria, and debris, followed by high-speed centrifugation at 12,000 × g for 30 min to pellet cell debris. The supernatant was filtered through 0.22 µm membrane, and subjected to ultracentrifugation at 135,000 × g for 70 min to obtain a crude BEV pellet, which was resuspended in 500 µL PBS and mixed with 2.5 mL 60% iodixanol solution. The mixture was loaded at the bottom of a discontinuous iodixanol density gradient consisting of 40%, 20%, 10% and 0% (PBS) iodixanol solutions. After performing density gradient ultracentrifugation at 160,000 × g for 15 h, a total of 4 mL BEV-containing fractions (F5-8) were collected, diluted in PBS, and ultracentrifuged once more to yield a purified BEV pellet. All of the above centrifugation procedures were carried out at 4°C, and ultracentrifugation was conducted in SW 32 Ti rotor from Beckman Coulter.

## 2.7 | Construction of mCherry *E. coli*

To create an *E. coli* strain expressing a red fluorescent mCherry fusion protein linked to the membrane protein OmpA, we employed the pET28a expression vector. The mCherry coding sequence was amplified using PCR, incorporating suitable restriction enzyme sites for subsequent cloning. Similarly, the OmpA coding sequence was amplified, excluding its stop codon to facilitate fusion with mCherry. The PCR products of mCherry and OmpA were sequentially cloned into the multiple cloning site of the pET28a vector using corresponding restriction enzymes, generating a translational fusion between the OmpA and mCherry sequences. EP tubes containing 50 µL of receptor bacteria were placed on wet ice and thawed. 1.5 µL of plasmid with mCherry was added to the receptor bacteria and mixed well; 51.5 µL of liquid was transferred to a pre-cooled rotor and incubated on ice for 5 min before being placed in the rotator at a voltage of 2500 V. The rotor was removed immediately after discharge and 0.5 mL of enhanced catabolic inhibition broth medium was added. Bacteria were transferred to 14 mL Falcon centrifuge tubes and incubated at 150 rpm for 1 h at 37°C; diluted the electrotransformed solution in a gradient and spread evenly on 100 mg/L ampicillin agar plates overnight at 37°C; selected red colonies of *E. coli* on Amp 100 plates incubated overnight, then inoculated on new plates (37°C, overnight); observed the overnight plates using IVIS, picked out clones with high fluorescence intensity, purify and preserved the strain (–80°C). HE sections were scored according to the simplified Geboes scale.

## 2.8 | Nanoparticle tracking analysis (NTA)

All samples were measured using NP100 membranes with parameters of 44.5 mm and 0.64 V voltage. The samples were diluted in 0.9% NaCl to an appropriate concentration and drawn into the pipe under identical settings (camera: 161 frames/s, sample volume: 1 mL). The detection threshold was calibrated to capture the maximum number of particles while ensuring that between 10 to 100 red crosses were tallied, and less than 10% were unassociated with distinct particles. Five videos, each typically 60 s in duration, were recorded. The video and output two dimensions were analyzed using the software of NTA (version 2.3, NanoSight).

## 2.9 | Transmission electron microscope (TEM)

The morphology of EVs was examined using a transmission electron microscope (Hitachi H-7500), following a previously described protocol (Choi et al., 2019). Briefly, isolated EVs were mixed with 4% paraformaldehyde and adsorbed onto carbon formvar-coated copper EM grids for 20 min. The samples were then rinsed with PBS and fixed with 1% glutaraldehyde for 2 min. Subsequently, the grids were washed with deionized water and stained with 1.5% uranyl acetate for 4 min. The air-dried grids were stored in a dark, dust-free environment until observation. Finally, images were captured and analyzed using a TEM.

## 2.10 | Nano-flow cytometry (nFCM)

EVs were incubated with Alexa Fluor 488-conjugated antibodies (mCherry, LPS or LTA) for 30 min at 37°C in the dark. The samples were then subjected to ultracentrifugation to remove unbound antibodies. All samples were prepared using the nFCM (Flow NanoAnalyzer, U30), adjusted to a concentration between  $10^7$ – $10^9$  particles/mL. The analysis parameters were set with a laser power of 15 mW, an SS Decay of 10%, a sampling pressure of 1.0 KPa, and a 1-min recording duration. Isotype controls matched to the given antibodies were also employed.

## 2.11 | Super-resolution imaging

For EVs visualization, mCherry *E. coli* EVs at a concentration of  $10^{10}$  particles/mL in Diluent C (10 mM Tris–HCl, pH 7.4; 150 mM NaCl; and 0.05% NaN<sub>3</sub>) were incubated with PKH67 (1  $\mu$ M) for 3 min, followed by the addition of 1% BSA for 5 min. The mixture was ultracentrifuged at  $120,000 \times g$  in PBS for 35 min to remove unbound dyes. Labeled BEVs were then resuspended in 100  $\mu$ L of PBS and diluted as necessary for subsequent experiments. For immunofluorescent labeling of LPS and LTA on EVs, 100  $\mu$ L of EV samples at a concentration of  $10^{10}$  particles/mL were combined with 1  $\mu$ L of primary antibody (LPS-AF647, LTA-AF647) and incubated at 37°C for 30 min. This was followed by washing with PBS ( $120,000 \times g$  for 35 min). The EVs were then stained with PKH67, as previously described, and washed with PBS. Imaging of bacteria and EVs was performed using a Nikon N-SIM microscope with the following excitation wavelengths: FITC/PKH67 at 488 nm, mCherry at 585 nm, and AF647 at 650 nm.

## 2.12 | Fluorescent imaging

mCherry *E. coli* was measured using IVIS spectrum (Caliper Life Sciences). mCherry *E. coli* were oral to mice (male, 4–6 weeks old, 14 day). The mCherry signals in the whole body of the mice were measured using IVIS spectrum (Caliper Life Sciences). Mice were sacrificed and the mCherry signals of various tissues including liver, lung, spleen, kidney and colon were measured. Living Image 3.1 software was used for measuring radiant efficiency.

## 2.13 | 16S ribosomal RNA gene sequencing

Stool DNA was extracted as described above by Stool DNA Extraction Kit (Qiagen) according to the manufacturer's recommendations. Sequencing was conducted as previously reported (Morrow et al., 2013). Data were processed using UPARSE and UTAX to generate operational taxonomic unit tables from 16S ribosomal RNA (rRNA) read data and make taxonomic assignments. Linear discriminant analysis effect size was applied to process 16S sequence data.

## 2.14 | Western blot

Lysates were prepared from bacteria, cells, and EVs. Protein concentration (20  $\mu$ g/ $\mu$ L) was determined using the BCA Protein Assay Kit (Beyotime). Loading buffer (Fdbio Science) was added to the samples, which were subsequently boiled under reducing

conditions. The samples were separated using SDS-PAGE gels (4-20%, Fdbio Science) and transferred to polyvinylidene difluoride (PVDF) membranes (Invitrogen). The samples were then probed with the following primary antibodies, as indicated in the figure legends: lipopolysaccharide (LPS; Abcam, 1:1000); lipoteichoic acid (LTA; Invitrogen, 1:1000); mCherry (Bioss, 1:1000); CD63, CD9 (Abcam, 1:1000) and Calnexin (Abcam, 1:20,000).

## 2.15 | H&E staining and histological score

Colon tissues for histological analysis were removed from the indicated mice and fixed in 4% paraformaldehyde immediately for 24 h. Then tissues were paraffin-embedded and sectioned. Slices were dewaxed by soaking with Xylene I for 20 min; Xylene II for 20 min; 100% ethanol I for 5 min; 100% ethanol II for 5 min; 75% ethanol for 5 min and rinsing with tap water. Stained sections with Hematoxylin solution for 3–5 min, rinsed with tap water. Then treated the section with Hematoxylin Differentiation solution, rinsed with tap water. Treated the section with Hematoxylin Scott Tap Bluing, rinsed with tap water. Dehydration with 85% ethanol for 5 min and 95% ethanol for 5 min; finally stained sections with Eosin dye for 5 min. Dehydrate sections again with 100% ethanol I for 5 min; 100% ethanol II for 5 min; 100% ethanol III for 5 min; Xylene I for 5 min; Xylene II for 5 min. Finally sealed with neutral gum and collected images by light microscopy.

## 2.16 | Fecal microbiota transplantation (FMT)

The fecal material was collected fresh from the aged (>18 months) and young (3 months) mice, homogenized in PBS, and then filtered through a 70  $\mu$ m cell strainer to remove large particulates. The resulting suspension was centrifuged briefly to sediment debris while keeping the bacterial component in suspension. The supernatant, containing the bacterial component, was then adjusted to a concentration of  $10^9$  CFU/mL. Over a period of three months, fecal microbiota were transplanted to young mice daily. Each young mouse received a daily gavage of 200  $\mu$ L.

## 2.17 | Wound healing assay

Intestinal epithelial cells (NCM460,  $5 \times 10^5$  cells/well) were seeded in 12-well plates and cultured until reaching 90% confluence. A scratch was created using a sterile pipette tip (200  $\mu$ L), and the wells were washed with PBS to eliminate detached cells. The cells were subsequently treated with purified BEVs (10  $\mu$ g/mL) at an appropriate concentration and incubated for 24 h. Images of the scratches were captured at 0 and 24 h with a light microscope, and wound closure was quantified.

## 2.18 | Invasion assay

Intestinal epithelial cells (NCM460) were pre-treated with purified BEVs (10  $\mu$ g/mL) for 24 h. After treatment, the cells were harvested, counted, and resuspended in serum-free medium. The invasion assay was carried out using Matrigel-coated transwell inserts placed in 24-well plates ( $5 \times 10^4$  cells/well). The upper chamber housed the treated cells, while the lower chamber contained medium with serum as a chemoattractant. Following a 24-h incubation period, non-invading cells were removed from the insert's upper surface, and the invading cells on the lower surface were fixed, stained, and counted.

## 2.19 | Statistical analysis

All quantitative data are expressed as mean  $\pm$  standard deviation (SD) unless otherwise indicated. For multiple comparisons, one-way analysis of variance (ANOVA) was used and corrected by Bonferroni. Statistical analysis was performed using GraphPad Prism 9.0. *P*-values of <0.05 were considered significant. \**P* < 0.05, \*\**P* < 0.01, \*\*\**P* 0.001, and \*\*\*\**P* < 0.0001.

# 3 | RESULTS

## 3.1 | Gut bacteria release BEVs into circulation

We first sought to confirm whether gut bacteria could release BEVs into the host bloodstream. In order to distinguish BEVs from host EVs, we attempted to specifically label BEVs. Given that BEVs carry components of the cell membrane when they are



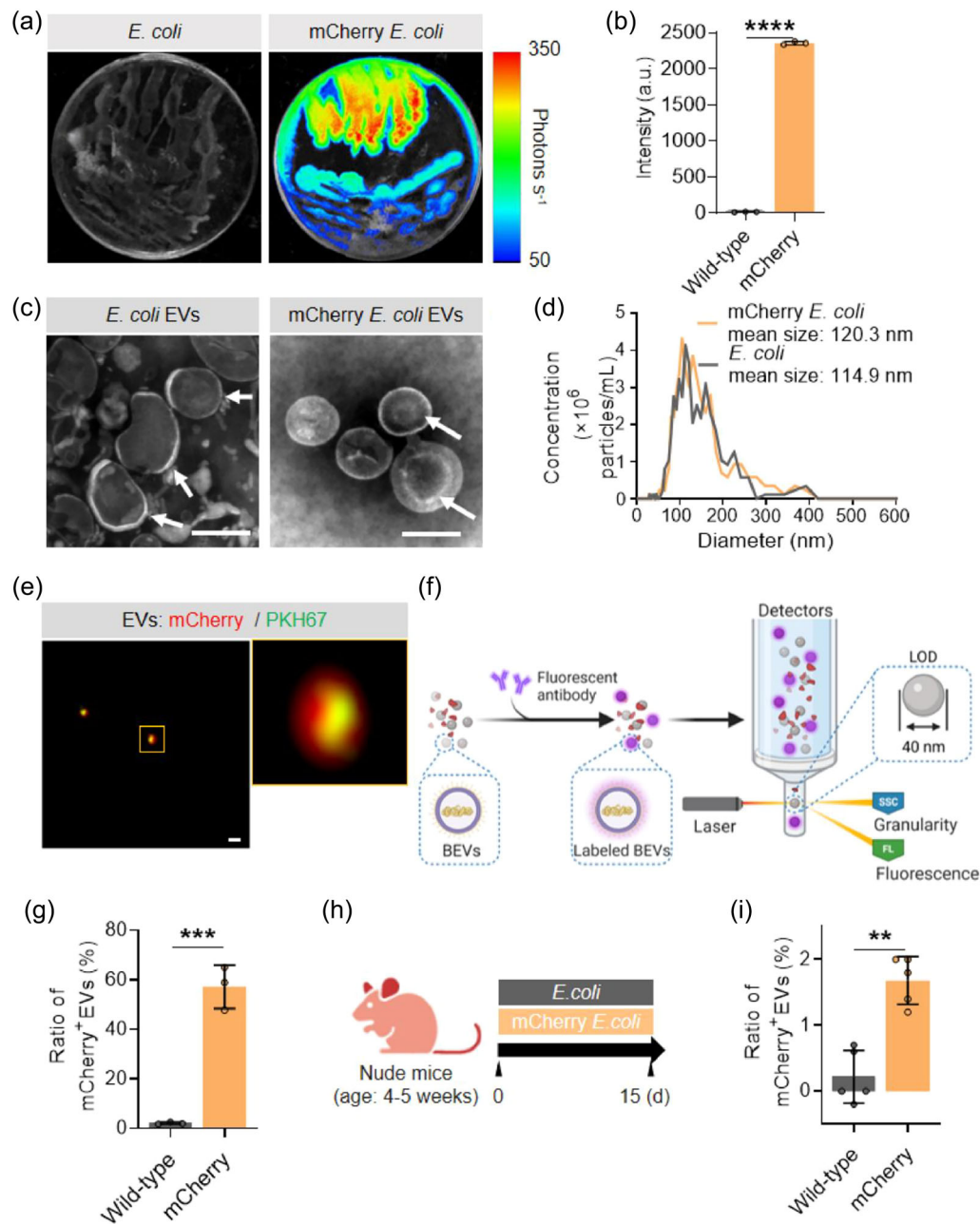


**FIGURE 1** Gut-derived BEVs are released to circulation. (a) Representative fluorescence images of *E. coli* and mCherry *E. coli* colonies; (b) Quantitative analysis of fluorescence intensities of *E. coli* and mCherry *E. coli* colonies; (c) TEM images of *E. coli*-EVs and mCherry *E. coli*-EVs. Scale bar: 100 nm; (d) Analysis of the size distributions of *E. coli*-EVs and mCherry *E. coli*-EVs by NTA; (e) Super-resolution imaging of mCherry *E. coli*-EVs (red) stained with PKH67 (green). Scale bar: 100 nm; (f) Schematic diagram of the nFCM platform for detection of single BEV; (g) Analysis of the labeling efficiency of mCherry to *E. coli* EVs by nFCM platform; (h) mCherry *E. coli* or *E. coli* were transplanted into 4- to 5-week-old mice and then housed in a controlled environment for 15 days before being euthanized ( $n = 5$ ); (i) The ratios of mCherry-positive EVs in circulating total EVs from the mice colonized with *E. coli* or mCherry *E. coli* after background corrected. Data are presented as mean  $\pm$  SEM of one experiment representative of three experiments; \* $P < 0.05$ , \*\* $P < 0.01$ , \*\*\* $P < 0.001$ , \*\*\*\* $P < 0.0001$ .

released, we designed a recombinant plasmid that is expected to express the fusion protein of fluorescent mCherry and OmpA (membrane protein) on the bacterial cell membrane. Following the transformation of the plasmid into *Escherichia coli* (*E. coli*) BL21 (Figure S1a), a substantial increase in red fluorescence was observed from both the bacterial colonies (Figure 1a,b) and the cell surface using fluorescent imaging (Figure S1b), indicating successful construction of the mCherry *E. coli*. We next compared the morphology, size distribution, and quantity of BEVs extracted from the medium of mCherry *E. coli* and the wild-type (WT) *E. coli* strains. Transmission electron microscopy (TEM) images from the both strains revealed the typical cup-shaped vesicles with similar morphology (Figure 1c, Figure S1c). No significant differences were found between the two strains in the concentrations

and size distributions (80–200 nm) of BEVs measured by nanoparticle tracking analysis (NTA) system (Figure 1d). Additionally, we found the presence of the LPS marker in the mCherry *E. coli* EVs and the *E. coli* EVs (Figure S10a). These data suggest that the genetically modified *E. coli* does not significantly affect its secreted BEVs.

We then investigated whether BEVs derived from mCherry *E. coli* also carry fluorescent label. Super-resolution imaging of the isolated BEVs showed that nanoparticles with red fluorescent mCherry were observed and mostly co-localized with the green fluorescence signals of PKH67 (membrane probe) (Figure 1e). The specific expression of mCherry on BEVs was also confirmed by immunoblotting (Figure S1d). These results indicated that the genetically modified *E. coli* we generated could stably release BEVs with fluorescent tags.

Since the analysis of trace bacterial vesicles in host samples requires highly sensitive and quantitative methods, we established a BEV detection platform using the nano-flow cytometry (nFCM). nFCM is an analytical technology by integrating light scattering with techniques for single-particle fluorescence detection in a sheathed flow (Tian et al., 2018). It has been shown to be capable of detecting nanoparticles as small as 40–200 nm (Tian et al., 2018). Using this platform and optimized experimental parameters, quantitative analysis of BEVs down to the single particle level was achieved (Figure 1f). Further measurement of the mCherry *E. coli* derived BEVs using this platform showed that up to 57.5% of particles carried mCherry fluorescence (Figure 1g), suggesting a high BEV labeling efficiency. We next fed the mice with the mCherry *E. coli* and WT strains to enable their colonization in the gut. After 15 days of feeding (Figure 1h), fluorescence in the mice abdomen in the mCherry *E. coli* treatment group were detected (Figure S2a). Further inspection of the organs *ex vivo* revealed that the signal was originated from the intestinal tract (Figure S2b), suggesting the colonization of mCherry *E. coli* in the gut. To investigate whether the BEVs derived from the gut mCherry *E. coli* can enter the circulation, total EVs from the blood of the mice were isolated, characterized by TEM and NTA (Figure S3a, b), and quantitatively analyzed using the nFCM platform. In the WT *E. coli* treating group, almost no fluorescent signal could be detected from the EVs. In contrast, a significant increase in the proportion of mCherry-positive (mCherry<sup>+</sup>) EVs (1%–2%) was detected in the mCherry *E. coli* treating group (Figure 1i). These results provide direct evidence that BEVs released by the gut bacteria can enter the peripheral circulation of the host.

### 3.2 | Identification of BEV markers for detection

The above findings prompted us to seek for BEV detection markers, as the genetic engineering strategy was not applicable to the real-world analysis. Ideal BEV markers should be universally expressed across different types of bacteria and not present in host cells. Based on these considerations, Lipopolysaccharide (LPS) and Lipoteichoic acid (LTA), two biomolecules that are widely expressed on gram-negative (G<sup>−</sup>) and gram-positive (G<sup>+</sup>) bacteria membranes, respectively, were selected to validate (Figure 2a). We extracted EVs from 3T3-L1 cells (mouse embryo fibroblasts), *E. coli* (G<sup>−</sup>) and *S. aureus* (G<sup>+</sup>) (Figure S4a,b, S10b–f) and found that LPS and LTA were only expressed on *E. coli*- and *S. aureus*-derived EVs (Figure 2b), respectively. Neither of them were present on EVs derived from 3T3-L1 cells (Figure 2b). Consistent results were observed from the immunofluorescence imaging of the EVs (Figure S4c–f).

To further quantify their expressions, we analyzed the EVs using the nFCM. EVs from more strains of G<sup>−</sup> bacteria (*M. catarrhalis*, *A. baumannii*, *P. aeruginosa*, and *E. coli*), G<sup>+</sup> bacteria (*E. faecium*, *S. pneumoniae*, *S. aureus*, and *S. epidermidis*), and from mammalian cell lines (MCF-7, A549, SMC, and 3T3-L1) were then isolated and determined by the nFCM. We found that the proportion of LPS-positive (LPS<sup>+</sup>) EVs from different strains of G<sup>−</sup> bacteria ranged from 35.7% to 60.5% (Figure 2c, Figure S5a), which was significantly higher than that from the mammalian cells (1.3%–1.7%), and G<sup>+</sup> bacteria strains (1.6%–2.0%) (Figure S5a,c). For the LTA-positive (LTA<sup>+</sup>) EVs, a high labeling proportion was observed from all the G<sup>+</sup> strains (34.8%–56.6%) (Figure 2d, Figure S5b), but almost undetectable from the G<sup>−</sup> bacteria (1.6%–2.2%) (Figure S5b,d) and the mammalian cells (0.6%–1.5%). These results demonstrate the potential of LPS and LTA as BEV markers for G<sup>−</sup> and G<sup>+</sup> bacteria, respectively. To further verify their specificity as BEV markers in host, we measured the ratio of LPS<sup>+</sup> or LTA<sup>+</sup> EVs in total EVs extracted from the blood of mice. Compared with the negative control germ-free (GF) mice, a significantly increased ratio of LPS<sup>+</sup> and LTA<sup>+</sup> EVs was detected in the blood of normal mice (Figure 2e,f), indicating their bacterial origin. Notably, when we treated the blood samples with the denaturant Triton X-100, specifically designed to disrupt EVs, the proportion of LPS<sup>+</sup> and LTA<sup>+</sup> particles dropped to approximately 5% of the levels observed prior to treatment (Figure S5e). The findings suggested that LPS<sup>+</sup> and LTA<sup>+</sup> particles are predominantly derived from BEV structures.

We next attempted to explore where the blood BEVs originate from. To test whether they mainly come from the intestinal tract, we administered a specific combination of antibiotics to C57BL/6J mice for 7 days to selectively target their gut microbiota. Owing to the limited absorption of certain antibiotics through oral administration, their impact on bacterial colonization in host sites outside the intestinal tract remains minimal (Yang et al., 2019) (Figure 2g). After 7 days of treatment, a significant reduction in the amounts of bacteria along with decreased microbiota diversity (Figure S6a–c) in the gut were detected by 16S rRNA sequencing and flow cytometry, suggesting the successful elimination of the gut microbiome. Compared to the control mice, elimination of gut bacteria led to a significantly decreased proportion both in the LPS<sup>+</sup> and LTA<sup>+</sup> EVs (Figure 2h,i) from the blood. These data indicate that circulating BEVs are mainly derived from the gut bacteria.

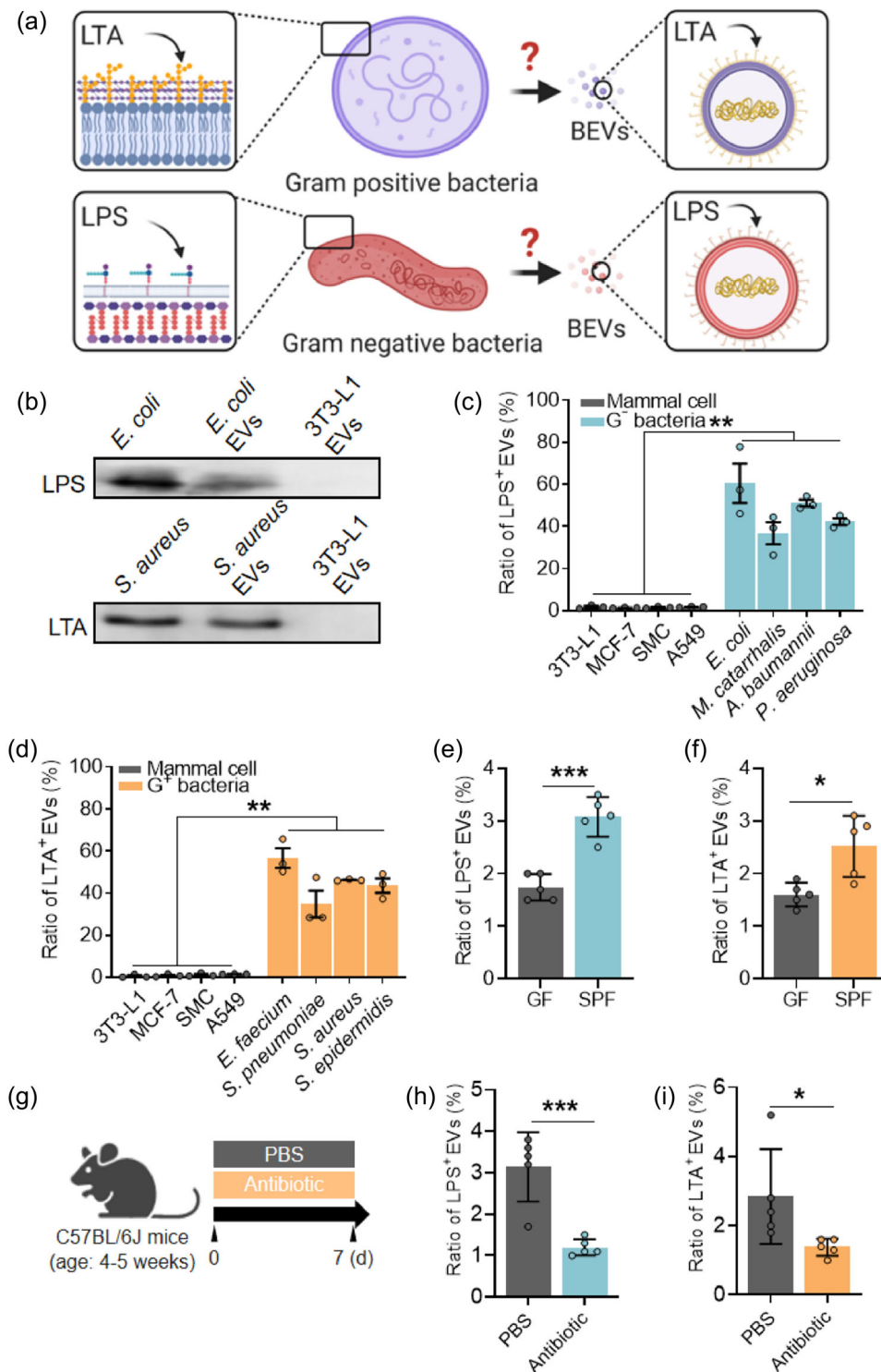


**FIGURE 2** Development of biomarkers for BEV detection. (a) Schematic diagram of the location of LPS and LTA molecules on the bacteria and BEVs; (b) Immunoblotting analysis of the LPS and LTA expression on representative G<sup>-</sup> bacteria (*E. coli*), G<sup>+</sup> bacteria (*S. aureus*), mammalian cells (3T3-L1 cells) and the BEV secreted by them; (c, d) The ratios of LPS<sup>+</sup> and LTA<sup>+</sup> EVs measured for EVs secreted by mammalian cells, G<sup>-</sup> bacteria and G<sup>+</sup> bacteria; (e, f) The ratios of LPS<sup>+</sup> and LTA<sup>+</sup> EVs in circulating total EVs from the GF or SPF mice; (g) Mice were implanted with antibiotic or PBS every day and then housed in a controlled environment for 7 days before being euthanized ( $n = 5$ ); (h, i) The ratios of LPS<sup>+</sup> and LTA<sup>+</sup> EVs in circulating total EVs from the mice with or without antibiotic treatment. Data are presented as mean  $\pm$  SEM of one experiment representative of three experiments for (c)–(i); \* $P < 0.05$ , \*\* $P < 0.01$ , \*\*\* $P < 0.001$ , \*\*\*\* $P < 0.0001$ .



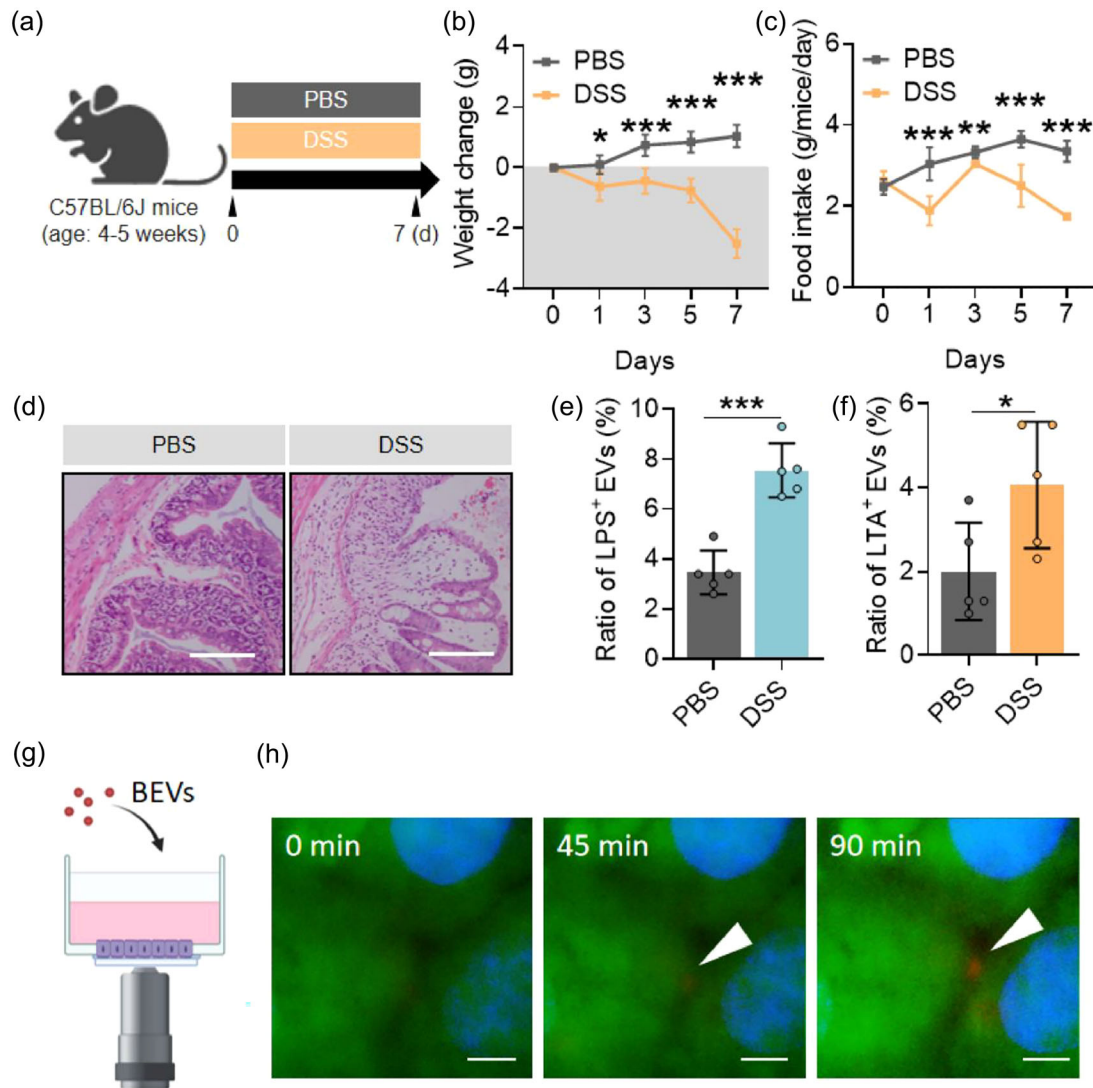


**FIGURE 3** Increase of circulating BEV abundance is associated with intestinal barrier dysfunction. (a) Four- to five-week-old mice were dealt with DSS or PBS every day and then housed in a controlled environment for 7 days before being euthanized; (b, c) The changes of food intake and weight of the mice dealt with DSS or PBS ( $n = 5$ ); (d) Hematoxylin and eosin (H&E) staining of the colon sections from the mice dealt with DSS or PBS. Scale bar: 100  $\mu$ m; (e, f) The ratios of LPS<sup>+</sup> and LTA<sup>+</sup> EVs in circulating total EVs from the mice dealt with DSS or PBS; (g) Schematic diagram of how BEVs (red) passing through epithelial monolayers (green); (h) Transmigration was observed simultaneously from the basal compartment (Bottom view) at indicated times after BEVs exposure. Scale bar: 2  $\mu$ m. Data are presented as mean  $\pm$  SEM of one experiment representative of three experiments for (a)–(f); \* $P < 0.05$ , \*\* $P < 0.01$ , \*\*\* $P < 0.001$ , \*\*\*\* $P < 0.0001$ .

### 3.3 | Gut BEVs enter into the circulatory system via intestinal barrier

We next asked how gut-derived BEVs enter the circulatory system. Given the significant role of intestinal barrier in health (García-Díaz et al., 2022), we speculated that intestinal barrier may be involved in the release of gut BEVs. To test this hypothesis, we used dextran sulfate sodium (DSS) to induce acute colitis in mice (Tian et al., 2020) (Figure 3a). After confirming the successful development of colitis by the decreased body weight, food intake of mice (Figure 3b,c) as well as pathological changes of the colon (Figure 3d, Figure S7a,b), we observed a significantly increased FITC-dextran and TNF- $\alpha$  levels in the mice serum after oral gavage (Figure S7c,d), which demonstrated the intestinal barrier dysfunction in the DSS-induced colitis model. Of note, we found that mice with dysfunction of intestinal barrier showed significantly higher levels of both LPS<sup>+</sup> and LTA<sup>+</sup> EVs compared to the control group (Figure 3e,f). These data showed that with the disruption of intestinal epithelial barrier, more BEVs will enter the bloodstream from the gut. To gain insight into the pathway by which BEVs penetrate the intestinal barrier, we labeled BEVs with mCherry and tracked their movement in a monolayer of cultured epithelial cells (NCM460) (Figure 3g). Confocal imaging showed that BEVs were able to cross the cell layer through intercellular space after treatment. The levels of BEVs in the medium from the lower compartment increased overtime (Figure 3h, Movie 1). Owing to their nanoscale size, composition, and

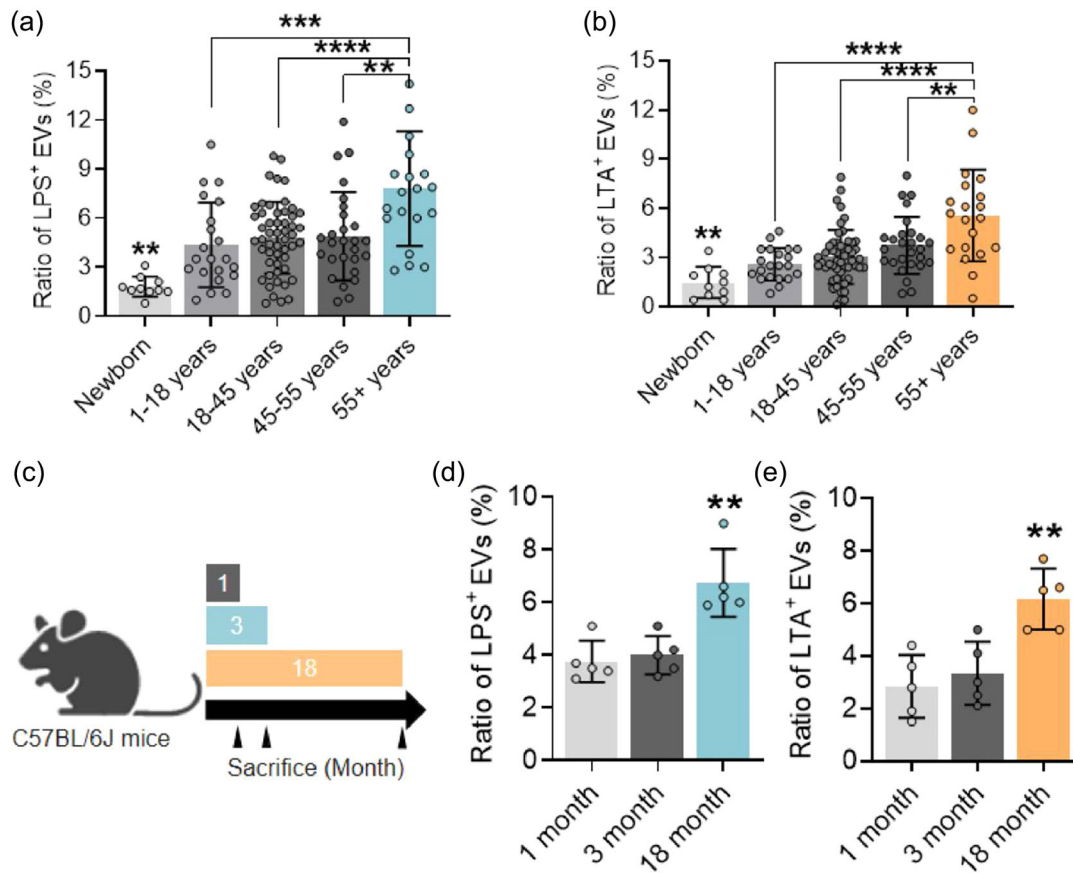


**FIGURE 4** Circulating BEV abundance is increased in an age-dependent way. (a, b) The ratios of LPS<sup>+</sup> and LTA<sup>+</sup> EVs in circulating total EVs from blood of different aged people; (c) Mice in 1 month, 3 months and 18 months were euthanized ( $n = 5$ ); (d, e) The ratios of LPS<sup>+</sup> and LTA<sup>+</sup> EVs in circulating total EVs from the mice in 1 month, 3 months and 18 months. Data are presented as mean  $\pm$  SEM of one experiment representative of three experiments for (c)–(e); \* $P < 0.05$ , \*\* $P < 0.01$ , \*\*\* $P < 0.001$ , \*\*\*\* $P < 0.0001$ .

ability to evade host immune responses, BEVs may display increased propensity for translocation across host cell membranes compared to other bacterial molecules, thereby enabling them to cross physiological barriers within the human body and exert regulatory effects on distant organs (Bhar et al., 2022; Niel et al., 2018; Schwechheimer & Kuehn, 2015).

### 3.4 | Circulating BEV levels change in an aging-related manner

The above findings prompt us to explore whether BEVs are present in human circulation. We analyzed serum from a sample set that included 130 healthy individuals aged 0–63 years (Table S1). We found that the lowest levels of LPS<sup>+</sup> and LTA<sup>+</sup> EVs were seen in the neonate group (<2%), whose concentrations were not statistically different from the negative control, suggesting that there were almost no detectable BEVs in the blood of the newborns (Figure 4a,b). This can be explained by the absence or extremely low amount of bacteria in the neonates (Morrow et al., 2013). BEV levels significantly increased at ~1 year of age and further increased (3%–4%) as individuals aged (1–55 years) (Figure 4a,b). A prominent increase of BEV level was observed (a fold change > 2) in the adults older than 55 years (Figure 4a,b). Consistent with these findings from human, we observed similar changes in mice (Figure 4c). BEV levels in the blood of mice were significantly increased in old age (18 months) compared to the young mice (1 months) and middle age (3 months) (Figure 4d,e). It has been reported that the intestinal barrier permeability of the elderly is higher than that of the younger (Leite et al., 2021). This was in agreement with our findings that the level of serum zonulin, a marker of the integrity of gut mucosal barrier, was significantly higher in old age than that from the young age individuals (Figure S8). Taken together, these results suggest that the amount of BEVs in the circulation significantly increased with aging across the lifespan and is related to an age-related increase in intestinal permeability.

To further investigate the impact of aged gut bacteria on the intestinal barrier disruption via BEVs, which leads to an increase in circulating BEVs, we transplanted fecal (FMT) from aged mice (18 months old) into young mice. Notably, we discovered that the intestinal barrier in young mice (3 months old) receiving the aged fecal transplant exhibited dysregulation (Figure S9a–c),

accompanied by a significant increase in circulating BEV abundance (Figure S9d). To further explore the effects of aged gut BEVs on the intestinal barrier dysfunction, we collected fecal samples from elderly (60 years and older) and young (18–45 years old) individuals and extracted EVs. Upon co-culturing the fecal EVs with intestinal epithelial cells (NCM460), we observed a significant reduction in cell proliferation (Figure S9e,f) and potential capability (Figure S9g,h) in the group treated with elderly fecal EVs. Consequently, these findings demonstrate that as age advances, an imbalance in gut microbiota and the release of BEVs compromise the intestinal barrier, facilitating the entry of more BEVs into circulation.

### 3.5 | Abundance of circulating BEVs was correlated with gut diseases

We next assessed whether the blood level of BEVs could be used as a biomarker for gastrointestinal diseases. A cohort of 30 patients with colitis included different levels of disease severity (mild  $n = 10$ , moderate  $n = 10$  and severe  $n = 10$ ) and 100 healthy donors was used to validate (Table S2). In patients with colitis, we found significant elevations in the serum levels of both LPS<sup>+</sup> and LTA<sup>+</sup> EVs (Figure 5a). Of note, the extent of increase was significant even in the colitis patients in the mild stage (Figure 5b,c). The receiver operating characteristic (ROC) curves showed that the LPS<sup>+</sup> and LTA<sup>+</sup> EVs levels could distinguish colitis patients from healthy donors with area under the curves (AUC) of 0.79 and 0.88, respectively. A higher diagnostics accuracy was showed (AUC: 0.90, 95% CI: 0.83–0.97) with the combination of these two EV markers together (Figure 5d). These data suggested that serum BEV levels may serve as potential markers for colitis. We next test the utility of BEVs in patients with colorectal cancer. Serum LPS<sup>+</sup> and LTA<sup>+</sup> EV analysis from a patient cohort revealed that cancer patients exhibited significantly elevated levels of LPS<sup>+</sup> EVs and LTA<sup>+</sup> EVs compared to healthy donors (Figure 5a). ROC curves demonstrated that serum LPS<sup>+</sup> and LTA<sup>+</sup> EVs revealed a classifier with AUC of 0.85 and 0.75, respectively, and a high AUC of 0.88 was achieved with the combined use of the two BEV markers (Figure 5g). Furthermore, higher serum BEV levels were significantly associated with more advanced stages of colorectal cancer, with a gradually increased level from 6% to 12% in the stage II to stage IV of cancer (Figure 5e,f), indicating the potential of BEV for tumor burden assessment. Collectively, our results demonstrated that circulating BEVs may be potential biomarkers of gut diseases.

## 4 | DISCUSSION

In recent years, BEVs have received extensive attention as an important mechanism of biological communication, especially in their role in microbiome-host interactions (Choi et al., 2019). Accurate and sensitive detection and quantification of BEVs is not only vital for understanding the interactions between bacteria and their host, but also opens up novel possibilities for disease diagnosis and treatment. However, due to the properties and abundance of BEVs, as well as technical limitations, reliable methods for BEV detection remain a challenge (Li et al., 2020). In this study, we demonstrate a highly efficient and sensitive BEV detection platform based on nFCM, and identify two potential BEV markers, LPS and LTA. Our findings provide novel tools and perspectives for revealing the distribution and functions of BEVs in the host circulatory system, and their roles in aging and intestinal diseases.

The identification of BEVs is a critical yet challenging endeavor in host. LPS and LTA, expressed in gram-negative and gram-positive bacteria, respectively, emerge as potential BEV markers (Kaparakis-Liaskos & Ferrero, 2015; Toyofuku et al., 2019). Nonetheless, the generalizability of LPS and LTA as biomarkers for BEV detection remains unconfirmed. Moreover, the amount of LPS or LTA present in BEVs released by different bacteria is inconsistent (Toyofuku et al., 2023). Without a platform for single-particle precision detection, BEVs with low marker abundance might be overlooked, thereby influencing the accuracy of the detection results (Choi et al., 2023). Our study authenticated these indicators, particularly within the framework of the nFCM platform. We offered quantifiable data on the presence of LPS<sup>+</sup> and LTA<sup>+</sup> EVs across diverse bacterial strains and mammalian cell. Overall, our advancement in single BEV particle detection accentuates the content of circulating BEVs under physiological and pathological conditions, establishing a crucial scientific basis for considering BEVs as viable biomarkers and prospective therapeutic agents.

Prior research has established that gut BEVs could penetrate into the circulatory system (Liu et al., 2021), and that circulating LPS<sup>+</sup> EVs exhibit a marked increase in patients with colitis (Tulkens et al., 2020). These findings imply a significant influence of our gut on the concentration of circulating BEVs. Herein, we found that circulating BEVs are mainly derived from gut bacteria, and they enter the circulatory system primarily via the intestinal barrier. We made an important observation that the amount of BEVs in the circulation significantly increases with aging, likely related to an age-related increase in intestinal permeability. Furthermore, aging is associated with disruptions in the composition of gut microbiota (Giannos et al., 2022), which in turn may compromise the intestinal barrier via enhanced BEV release, subsequently intensifying the levels of circulating BEVs in individuals. This mechanism may provide an explanation for the potential role of circulating BEVs as markers for conditions characterized by increased intestinal barrier permeability, such as aging and colitis.

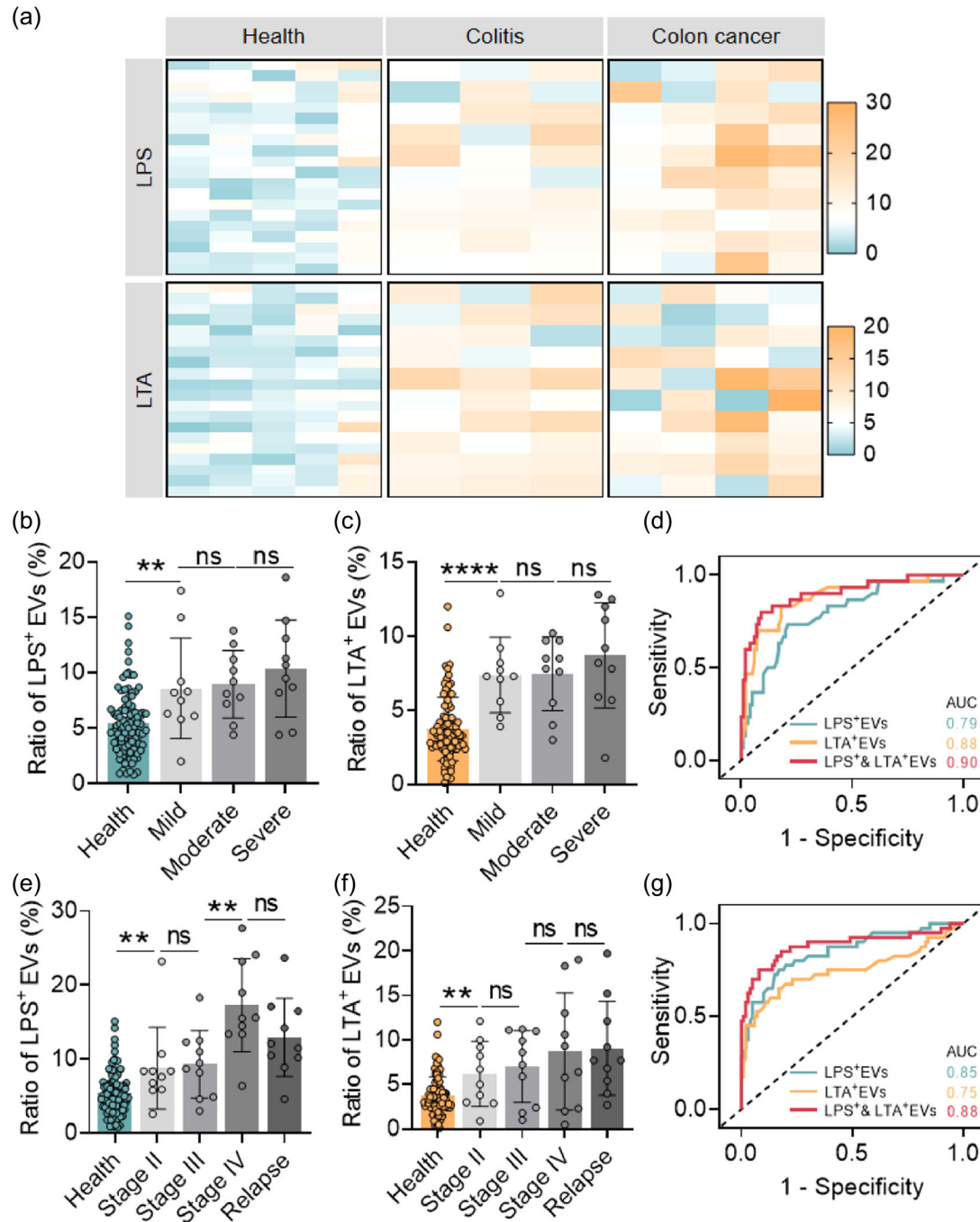


**FIGURE 5** Circulating BEV abundance increase in patients with intestinal diseases. (a) Heat map for comparing the ratios of LPS<sup>+</sup> and LTA<sup>+</sup> EVs in circulating total EVs from healthy donors and patients with colitis and colon cancer; (b, c) The ratios of LPS<sup>+</sup> and LTA<sup>+</sup> EVs in circulating total EVs from healthy donors and patients with colitis at different stages; (d) ROC curves between healthy donors and colitis patients assessed by the ratios of LPS<sup>+</sup> and LTA<sup>+</sup> EVs; (e, f) The ratios of LPS<sup>+</sup> and LTA<sup>+</sup> EVs in circulating total EVs from healthy donors and patient with colon cancer at different stages; (g) ROC curves between healthy donors and colorectal cancer patients assessed by the ratios of LPS<sup>+</sup> and LTA<sup>+</sup> EVs. Data are presented as mean  $\pm$  SEM; \* $P$  < 0.05, \*\* $P$  < 0.01, \*\*\* $P$  < 0.001, \*\*\*\* $P$  < 0.0001.

However, it is unclear whether other factors, such as diet or the use of medication, could influence the amount of circulating BEVs in the host. In addition, the exact mechanism of how BEVs cross the intestinal barrier remains to be fully elucidated. Notably, our method for serum EV isolation minimized interference, but it doesn't entirely eliminate contaminants like lipoproteins. This underscores the imperative to refine EV isolation techniques, aiming to bolster large-scale clinical validations of BEVs' relevance in disease diagnosis and treatment. Despite these limitations, our findings offer exciting new directions for future research. The observation that BEVs enter the bloodstream and their levels increase with aging highlights a potential role



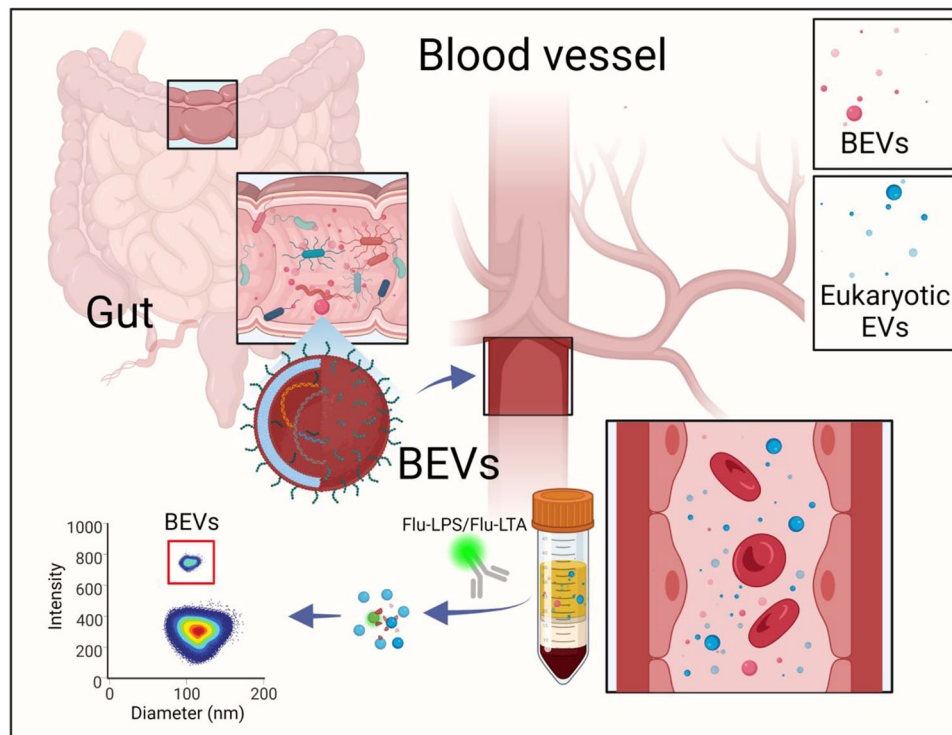
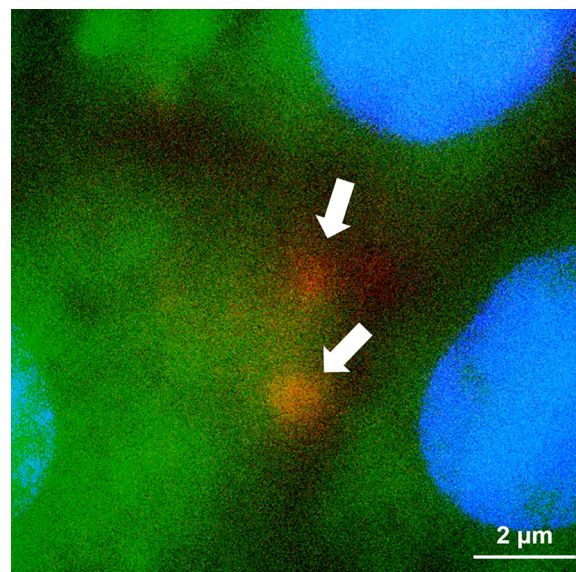


**FIGURE 6** Here, we developed a single-vesicle analytical platform that enabled BEV detection in complex biological samples of host. Using this platform, we found the presence of BEVs in the host circulation and they were mainly derived from gut microbes. We showed that the levels of circulating BEVs in humans significantly increased with aging due to an age-related increase in intestinal permeability. Significantly different levels of BEVs in blood were also found in patients with colorectal cancer and colitis.



**Movie 1** The passage of BEVs (highlighted in red) through epithelial monolayers (visualized in green).

for BEVs in aging-related changes in physiology, which should be further investigated. Furthermore, the potential of BEVs as novel biomarkers for gut-related diseases such as colitis and colorectal cancer opens a new avenue for non-invasive diagnosis and tracking of these diseases. Taken together, our work adds significantly to the existing body of knowledge about the role and significance of BEVs, providing fresh insights that can be used to guide future research and clinical applications.



## 5 | CONCLUSION

In summary, we have identified markers that can distinguish bacterial EVs from host-derived EVs. Combining with a single-vesicle analytical platform, we confirmed the stable presence of BEVs in blood samples from mice and humans and revealed their gut bacterial biogenesis. We discovered a pattern of changes in blood BEVs that increased across the human lifespan and was associated with age-related increased intestinal permeability. Of clinical value, we showed that circulating BEVs may serve as a potential biomarker for intestinal diseases (Figure 6). Overall, our findings provide valuable insights into the circulating BEVs in health and diseases. Considering the propensity of BEVs to translocate across host cell membranes, causing pathological changes more readily than other bacterial molecules, further exploration of circulating BEVs could illuminate the pathogenesis of microbiome-associated human diseases. Our methodology could thus serve as a platform for future research delving into the specific characteristics of various bacterial BEVs.

## AUTHOR CONTRIBUTIONS

Zihao Ou and Bo Situ designed, performed, and analyzed in vivo experiments. Zihao Ou performed and analysed the vesicle purification, EV imaging, ELISA, immunoblot and mouse experiments. Xinyue Huang and Yicong Xue generated the GF mice. Xiaojing He and Qianbei Li supervised experiments and provided critical reagents. Zihao Ou, and Bo Situ wrote the paper, which other authors commented on. Bo Situ and Lei Zheng and Qian Wang supervised the project.

## ACKNOWLEDGEMENTS

This work was supported by the National Science Fund for Distinguished Young Scholars (82025024); the National Key R&D Program of China (2021YFA1300604); the National Natural Science Foundation of China (82302593, 82272438 and 82002245); the Post-doctoral Science Foundation (2022M720059); the Outstanding Youths Development Scheme of Nanfang Hospital, Southern Medical University (2022J001); the Natural Science Foundation of Guangdong Province (2021A1515011639, 2023A1515012512); the Major State Basic Research Development Program of Natural Science Foundation of Shandong Province in China (ZR2020ZD11).

## CONFLICT OF INTEREST STATEMENT

All other authors declare no competing interests.

## DATA AVAILABILITY STATEMENT

The data that support the findings of this study are available from the corresponding author upon reasonable request.

## ORCID

Zihao Ou  <https://orcid.org/0000-0001-8722-7205>

Qian Wang  <https://orcid.org/0000-0002-0299-4462>

Lei Zheng  <https://orcid.org/0000-0003-2576-8780>

## REFERENCES

- Amin, M. B., Greene, F. L., Edge, S. B., Compton, C. C., Gershenwald, J. E., Brookland, R. K., Meyer, L., Gress, D. M., Byrd, D. R., & Winchester, D. P. (2017). The eighth edition AJCC cancer staging manual: Continuing to build a bridge from a population-based to a more “personalized” approach to cancer staging. *CA: A Cancer Journal for Clinicians*, 67, 93.
- Ashrafian, F., Shahriary, A., Behrouzi, A., Moradi, H. R., Keshavarz Azizi Raftar, S., Lari, A., Hadifar, S., Yaghoobfar, R., Ahmadi Badi, S., Khatami, S., Vaziri, F., & Siadat, S. D. (2019). *Akkermansia muciniphila*-Derived extracellular vesicles as a mucosal delivery vector for amelioration of obesity in mice. *Frontiers in Microbiology*, 10, 2155.
- Atreya, R., & Siegmund, B. (2021). Location is important: Differentiation between ileal and colonic Crohn’s disease. *Nature Reviews Gastroenterology & Hepatology*, 18, 544.
- Bhar, S., Zhao, G., Bartel, J. D., Sterchele, H., Del, A. M., Emerson, L. E., Edelmann, M. J., & Jones, M. K. (2022). Bacterial extracellular vesicles control murine norovirus infection through modulation of antiviral immune responses. *Frontiers in Immunology*, 13, 909949.
- Bittel, M., Reichert, P., Sarfati, I., Dressel, A., Leikam, S., Uderhardt, S., Stolzer, I., Phu, T. A., Ng, M., Vu, N. K., Tenzer, S., Distler, U., Wirtz, S., Rothhammer, V., Neurath, M. F., Raffai, R. L., Günther, C., & Momma, S. (2021). Visualizing transfer of microbial biomolecules by outer membrane vesicles in microbe-host-communication in vivo. *Journal of Extracellular Vesicles*, 10, e12159.
- Carter, M. J., Lobo, A. J., Travis, S. P. L., & IBD Section, British Society of Gastroenterology. (2004). Guidelines for the management of inflammatory bowel disease in adults. *Gut*, 53(Suppl 5), V1.
- Cecil, J. D., Sirisaengtaksin, N., O’Brien-Simpson, N. M., & Krachler, A. M. (2019). Outer membrane vesicle-host cell interactions. *Microbiology Spectrum*, 7, <https://doi.org/10.1128/microbiolspec.PSIB-0001-2018>
- Chen, C.-Y., Rao, S.-S., Yue, T., Tan, Y.-J., Yin, H., Chen, L.-J., Luo, M.-J., Wang, Z., Wang, Y.-Y., Hong, C.-G., Qian, Y.-X., He, Z.-H., Liu, J.-H., Yang, F., Huang, F.-Y., Tang, S.-Y., & Xie, H. (2022). Glucocorticoid-induced loss of beneficial gut bacterial extracellular vesicles is associated with the pathogenesis of osteonecrosis. *Science Advances*, 8, eabg8335.
- Choi, D., Montermini, L., Jeong, H., Sharma, S., Meehan, B., & Rak, J. (2019). Mapping subpopulations of cancer cell-derived extracellular vesicles and particles by nano-flow cytometry. *ACS Nano*, 13(9), 10499.

- Choi, Y., Park, H. S., & Kim, Y. K. (2023). Extracellular vesicles: A candidate molecule for the diagnosis and treatment of allergic diseases. *Allergy, Asthma & Immunology Research*, 15(3), 279.
- Erttmann, S. F., Swacha, P., Aung, K. M., Brindelfalk, B., Jiang, H., Härtlova, A., Uhlin, B. E., Wai, S. N., & Gekara, N. O. (2022). The gut microbiota prime systemic antiviral immunity via the cGAS-STING-IFN-I axis. *Immunity*, 55, 847.
- Fassarella, M., Blaak, E. E., Penders, J., Nauta, A., Smidt, H., & Zoetendal, E. G. (2021). Gut microbiome stability and resilience: elucidating the response to perturbations in order to modulate gut health. *Gut*, 70, 595.
- Frost, F., Kacprowski, T., Rühlemann, M., Pietzner, M., Bang, C., Franke, A., Nauck, M., Völker, U., Völzke, H., Dörr, M., Baumbach, J., Sendler, M., Schulz, C., Mayerle, J., Weiss, F. U., Homuth, G., & Lerch, M. M. (2021). Long-term instability of the intestinal microbiome is associated with metabolic liver disease, low microbiota diversity, diabetes mellitus and impaired exocrine pancreatic function. *Gut*, 70, 522.
- García-Díaz, M., Cendra, M. D. M., Alonso-Roman, R., Urdániz, M., Torrents, E., & Martínez, E. (2022). Mimicking the intestinal host-pathogen interactions in a 3D in vitro model: The role of the mucus layer. *Pharmaceutics*, 14, 1552.
- Giannos, P., Prokopidis, K., Isanejad, M., & Wright, H. L. (2022). Markers of immune dysregulation in response to the ageing gut: Insights from aged murine gut microbiota transplants. *BMC Gastroenterology [Electronic Resource]*, 22(1), 533.
- Gul, L., Modos, D., Fonseca, S., Madgwick, M., Thomas, J. P., Sudhakar, P., Booth, C., Stentz, R., Carding, S. R., & Korcsmaros, T. (2022). Extracellular vesicles produced by the human commensal gut bacterium *Bacteroides thetaiotaomicron* affect host immune pathways in a cell-type specific manner that are altered in inflammatory bowel disease. *Journal of Extracellular Vesicles*, 11, e12189.
- Han, N. D., Cheng, J., Delannoy-Bruno, O., Webber, D., Terrapon, N., Henrissat, B., Rodionov, D. A., Arzamasov, A. A., Osterman, A. L., Hayashi, D. K., Meynier, A., Vinoy, S., Desai, C., Marion, S., Barratt, M. J., Heath, A. C., & Gordon, J. I. (2022). Microbial liberation of N-methylserotonin from orange fiber in gnotobiotic mice and humans. *Cell*, 185, 2495.
- Hod, K., & Ringel, Y. (2016). Probiotics in functional bowel disorders. *Best Practice & Research. Clinical Gastroenterology*, 30, 89.
- Janda, M., & Robatzek, S. (2022). Extracellular vesicles from phytobacteria: Properties, functions and uses. *Biotechnology Advances*, 58, 107934.
- Jiang, L., Driedonks, T. A. P., Jong, W. S. P., Dhakal, S., Bart van den Berg van Saparoea, H., Sitaras, I., Zhou, R., Caputo, C., Littlefield, K., Lowman, M., Chen, M., Lima, G., Gololobova, O., Smith, B., Mahairaki, V., Richardson, M. R., Mulka, K. R., Lane, A. P., Klein, S. L., ... Witwer, K. W. (2022). A bacterial extracellular vesicle-based intranasal vaccine against SARS-CoV-2 protects against disease and elicits neutralizing antibodies to wild-type and Delta variants. *Journal of Extracellular Vesicles*, 11, e12192.
- Kaparakis-Liaskos, M., & Ferrero, R. L. (2015). Immune modulation by bacterial outer membrane vesicles. *Nature Reviews Immunology*, 15, 375.
- Lee, J.-Y., Tsolis, R. M., & Bäuml, A. J. (2022). The microbiome and gut homeostasis. *Science*, 377, eabp9960.
- Leite, G., Pimentel, M., Barlow, G. M., Chang, C., Hosseini, A., Wang, J., Parodi, G., Sedighi, R., Rezaie, A., & Mathur, R. (2021). Age and the aging process significantly alter the small bowel microbiome. *Cell Reports*, 36, 109765.
- Li, M., Zhou, H., Yang, C., Wu, Y., Zhou, X., Liu, H., & Wang, Y. (2020). Bacterial outer membrane vesicles as a platform for biomedical applications: An update. *Journal of Controlled Release*, 323, 253.
- Liu, J. H., Chen, C. Y., Liu, Z. Z., Luo, Z. W., Rao, S. S., Jin, L., Wan, T. F., Yue, T., Tan, Y. J., Yin, H., Yang, F., Huang, F. Y., Guo, J., Wang, Y. Y., Xia, K., Cao, J., Wang, Z. X., Hong, C. G., Luo, M. J., ... Xie, H. (2021). Extracellular vesicles from child gut microbiota enter into bone to preserve bone mass and strength. *Advancement of Science*, 8(9), 2004831.
- Møller, S. H., Hsueh, P.-C., Yu, Y.-R., Zhang, L., & Ho, P.-C. (2022). Metabolic programs tailor T cell immunity in viral infection, cancer, and aging. *Cell Metabolism*, 34, 378.
- Morrow, A. L., Lagomarcino, A. J., Schibler, K. R., Taft, D. H., Yu, Z., Wang, B., Altaye, M., Wagner, M., Gevers, D., Ward, D. V., Kennedy, M. A., Huttenhower, C., & Newburg, D. S. (2013). Early microbial and metabolomic signatures predict later onset of necrotizing enterocolitis in preterm infants. *Microbiome*, 1, 13.
- Niel, G. V., Angelo, G. D., & Raposo, G. (2018). Shedding light on the cell biology of extracellular vesicles. *Nature Reviews Molecular Cell Biology*, 19(4), 213.
- Ou, Z., Deng, L., Lu, Z., Wu, F., Liu, W., Huang, D., & Peng, Y. (2020). Protective effects of *Akkermansia muciniphila* on cognitive deficits and amyloid pathology in a mouse model of Alzheimer's disease. *Nutrition & Diabetes*, 10, 12.
- Schwechheimer, C., & Kuehn, M. J. (2015). Outer-membrane vesicles from Gram-negative bacteria: biogenesis and functions. *Nature Reviews Microbiology*, 13(10), 605.
- Serger, E., Luengo-Gutierrez, L., Chadwick, J. S., Kong, G., Zhou, L., Crawford, G., Danzi, M. C., Myridakis, A., Brandis, A., Bello, A. T., Müller, F., Sanchez-Vassopoulos, A., De Virgiliis, F., Liddell, P., Dumas, M. E., Strid, J., Mani, S., Dodd, D., & Di Giovanni, S. (2022). The gut metabolite indole-3 propionate promotes nerve regeneration and repair. *Nature*, 607, 585.
- Tan, A. H., Lim, S. Y., & Lang, A. E. (2022). The microbiome-gut-brain axis in Parkinson disease—From basic research to the clinic. *Nature Reviews Neurology*, 18, 476.
- Tang, W. H. W., Li, D. Y., & Hazen, S. L. (2019). Dietary metabolism, the gut microbiome, and heart failure. *Nature Reviews Cardiology*, 16, 137.
- Tian, M., Wang, X., Sun, J., Lin, W., Chen, L., Liu, S., Wu, X., Shi, L., Xu, P., Cai, X., & Wang, X. (2020). IRF3 prevents colorectal tumorigenesis via inhibiting the nuclear translocation of  $\beta$ -catenin. *Nature Communications*, 11, 5762.
- Tian, Y., Ma, L., Gong, M., Su, G., Zhu, S., Zhang, W., Wang, S., Li, Z., Chen, C., Li, L., Wu, L., & Yan, X. (2018). Protein profiling and sizing of extracellular vesicles from colorectal cancer patients via flow cytometry. *ACS Nano*, 12, 671.
- Toyofuku, M., Nomura, N., & Eberl, L. (2019). Types and origins of bacterial membrane vesicles. *Nature Reviews Microbiology*, 17, 13.
- Toyofuku, M., Schild, S., Liaskos, M. K., & Eberl, L. (2019). *Nature Reviews Microbiology*, 10, 1038.
- Tulkens, J., Vergauwen, G., Van Deun, J., Geerickx, E., Dhondt, B., Lippens, L., De Scheerder, M.-A., Miinalainen, I., Rappu, P., De Geest, B. G., Vandecasteele, K., Laukens, D., Vandekerckhove, L., Denys, H., Vandesompele, J., De Wever, O., & Hendrix, A. (2020). Increased levels of systemic LPS-positive bacterial extracellular vesicles in patients with intestinal barrier dysfunction. *Gut*, 69, 191.
- Turner, L., Bitto, N. J., Steer, D. L., Lo, C., D'Costa, K., Ramm, G., Shambrook, M., Hill, A. F., Ferrero, R. L., & Kaparakis-Liaskos, M. (2018). *Helicobacter pylori* outer membrane vesicle size determines their mechanisms of host cell entry and protein content. *Frontiers in Immunology*, 9, 1466.
- Wen, M., Wang, J., Ou, Z., Nie, G., Chen, Y., Li, M., Wu, Z., Xiong, S., Zhou, H., Yang, Z., Long, G., Su, J., Liu, H., Jing, Y., Wen, Z., Fu, Y., Zhou, T., Xie, H., Guan, W., ... Zheng, L. (2023). Bacterial extracellular vesicles: A position paper by the microbial vesicles task force of the Chinese society for extracellular vesicles. *Interdiscip Med*, 1, e20230017.
- Yang, D., Chen, X., Wang, J., Lou, Q., Lou, Y., Li, L., Wang, H., Chen, J., Wu, M., Song, X., & Qian, Y. (2019). Dysregulated lung commensal bacteria drive Interleukin-17B production to promote pulmonary fibrosis through their outer membrane vesicles. *Immunity*, 50, 692.

## SUPPORTING INFORMATION

Additional supporting information can be found online in the Supporting Information section at the end of this article.

**How to cite this article:** Ou, Z., Situ, B., Huang, X., Xue, Y., He, X., Li, Q., Ou, D., He, B., Chen, J., Huang, Y., Deng, L., Zhang, M., Wang, Q., & Zheng, L. (2023). Single-particle analysis of circulating bacterial extracellular vesicles reveals their biogenesis, changes in blood and links to intestinal barrier. *Journal of Extracellular Vesicles*, 12, e12395. <https://doi.org/10.1002/jev2.12395>